

Rock physics templates - a tutorial

Satinder Chopra¹, Ritesh Kumar Sharma¹, and Neeraj Kumar²

INTRODUCTION TO ROCK PHYSICS TEMPLATES

Rock physics templates (or RPTs, as they are commonly referred to) are a graphical framework used in reservoir geophysics to interpret elastic properties of rocks typically P-impedance (I_P) , and V_PV_S - in terms of lithology and fluid content. Alternative template domains have been used by practitioners, e.g., Pimpedance versus Poisson's ratio, P-impedance versus El, Lambda-rho versus Mu-rho. It provides a visual and quantitative tool to link seismic attributes with reservoir properties using rock physics models. As an example, in Figure 1a, we show an RPT overlaid on the crossplot between the P-impedance and V_P/V_S for well data, for an interval comprising the broad zone of interest in the Hoop Fault Complex area in the Barents Sea including the prospective Mid Triassic sandstone channels. The cluster points are color coded with porosity values ranging from 5% to 25%. The clusters of points with low impedance and low V_P/V_S exhibit high porosity and high gas saturation and are enclosed in red and purple ellipses. In Figure 1b, we show a similar crossplot for the P impedance and V_P/V_S derived from prestack simultaneous impedance inversion without frequency balancing, with overlaid RPTs. Notice that the cluster of points has an overall shape that is similar to the one seen in the crossplot shown in Figure 1a from well data. The drawback we see is that the cluster points within the red and purple ellipses are not spread out. In Figure 1c, we show an equivalent crossplot from the two attributes derived from prestack simultaneous impedance inversion with frequency balancing. Now we see a good spread of cluster points within the red and purple ellipses.

The RPT generated in Figure 1 is for a restricted interval of interest including the sandstones, but if the same RPT is generated for a larger interval comprising different lithologies, then besides the sandstone, other lithologies will show up as we will see in the next section. Additionally, depth trends could also affect the RPTs (Avseth, 2025).

The motivation behind writing this tutorial is to explain how these templates are constructed and bring clarity on the interpretation of this useful tool. The approach adopted in the generation of the templates is to make use of rock physics relations for quantifying the geophysical response of rock and fluid properties. Consequently, we begin this tutorial with a brief description of the common lithologies we deal with and the relevant descriptions of their rock physics analysis, before we go on to the discussion of the rock physics templates.

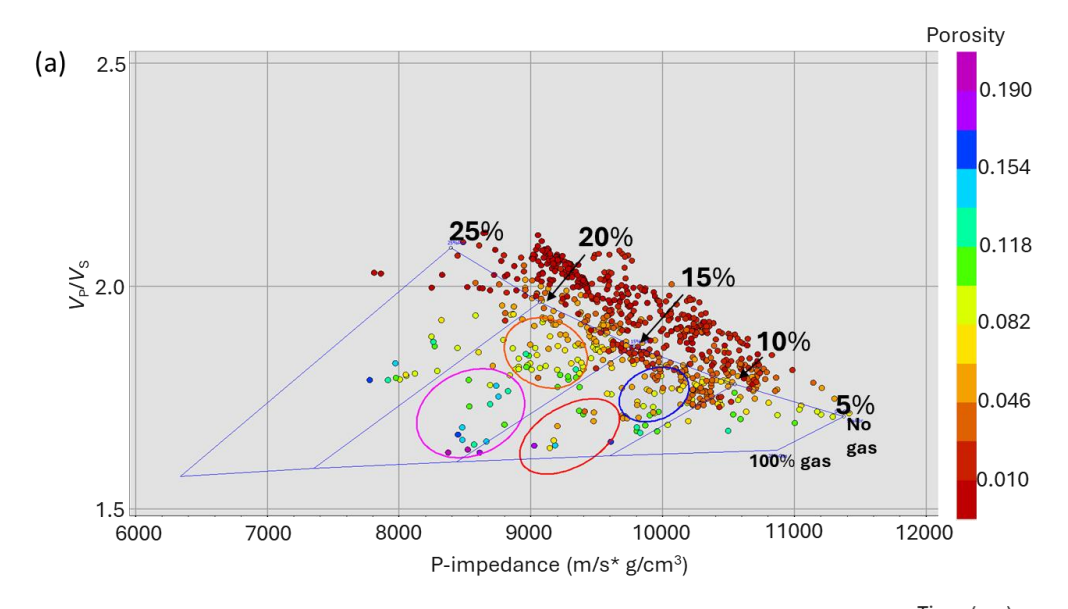
For a siliciclastic environment, usually the lithologies of interest are shale, shaly sands and clean sands. For sandy systems, the quartz-rich (arenite), feldspar-rich (arkose) sands need to be distinguished, and they have different elastic properties. Furthermore, distinction needs to be made between unconsolidated sands and cemented sandstones (i.e., diagenesis). The latter refers to solid rocks where cement is deposited at the sand grain contacts. This cement is often silica (quartz), calcite, or clay minerals, and is elastic. Its presence affects the stiffness, strength, porosity and the overall behaviour of the rock. Cementation generally reduces porosity by filling the pores between the grains. Stronger cement bonds lend higher compressive strength and make the rock resistant to deformation.

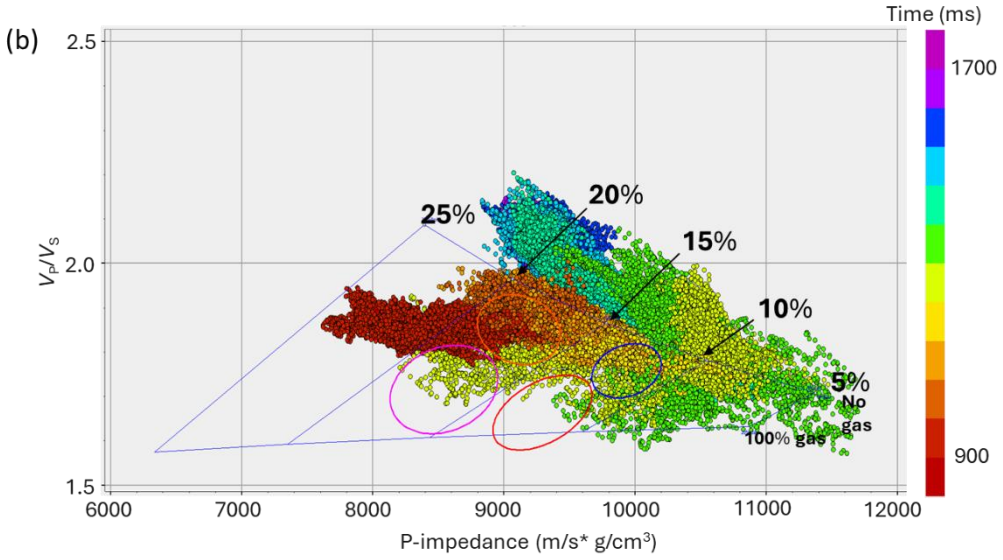
For carbonates, the lithologies of interest are limestone, dolostone, coguina and chalk.

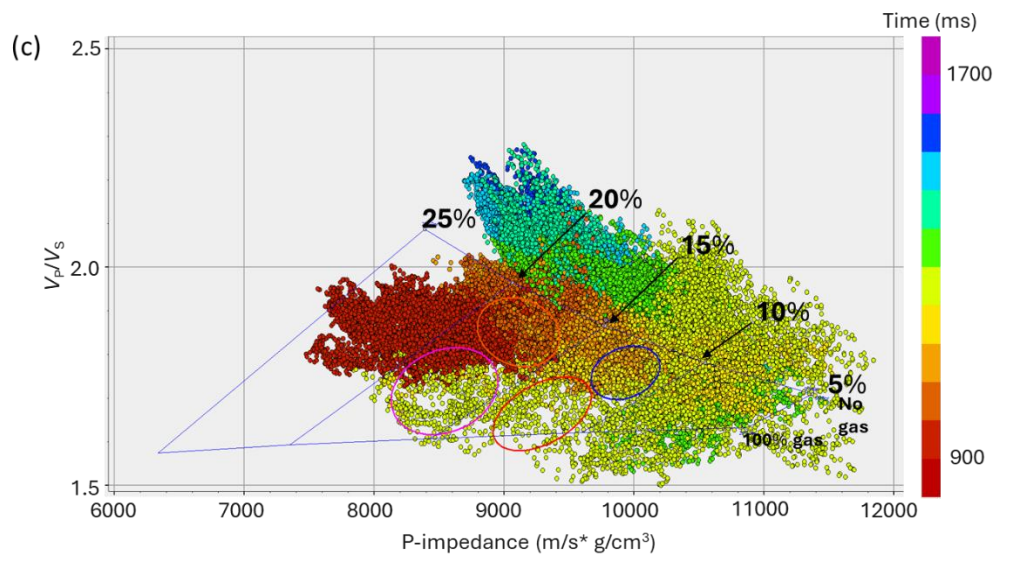
Besides these, the water depth or the depth of the formation of interest determine the effective pressure, pore pressure and lithostatic pressure. Pore pressure is important for the calculation of fluid properties and to determine the effective stress on the grain contacts of the rock frame carrying the overburden. Porosity reduction associated with rock compaction and diagenesis are directly related to burial depth. At greater depths quartz-rich sands tend to be quartz cemented, whereas smectite-rich shales will go through illitization and release of bound water.

¹SamiGeo, Calgary, Canada. Email: Satinder.Chopra@samigeo.com; Ritesh.Sharma@samigeo.com

²Canacol Energy Ltd., Calgary, Canada. Email: nkumar@canacolenergy.com







GEOHORIZONS, Vol. 30, No. 1, June 2025 © SPG India. All rights reserved.

Figure 1: (a) Crossplot between the P-impedance and $V_P V_S$ for well data, and for the broad zone of interest, with an RPT overlaid on it. The cluster of points with low impedance and low $V_P V_S$ exhibit high porosity and high gas saturation and are enclosed in red and purple ellipses. (b) Crossplot between the P-impedance and $V_P V_S$ derived from seismic prestack simultaneous impedance inversion for the same interval. The same RPT shown in (a) is overlaid on it. The cluster of points exhibit an overall shape similar to the cluster we see for well data, but they do not seem scattered enough within the red and purple ellipses, (c) Crossplot between the P-impedance and V_P√V_S derived from seismic simultaneous prestack impedance inversion after frequency enhancement, and for the same interval. The same RPT shown in (a) is overlaid on it. The cluster of points exhibits an overall shape similar to the cluster we see for well data, but they are now well-scattered within the red and purple ellipses, and thus they offer a more accurate interpretation. (After Chopra et al., 2017)

ROCK PHYSICS ANALYSIS

Any rock physics analysis for such rock formations will need to consider many of the above relevant aspects.

Given the measurement of V_P and V_S for a given saturation, it is possible to calculate bulk and shear modulus, using the following relationships.

$$V_{\rm P} = \sqrt{\frac{\kappa_{sat} + \frac{4}{3}\mu_{sat}}{\rho_b}},\tag{1}$$

$$\kappa_{sat} = \rho_b V_P^2 - \frac{4}{3} \mu_{sat} . \tag{2}$$

$$V_{\rm S} = \sqrt{\frac{\mu_{\rm Sat}}{\rho_b}},\tag{3}$$

and
$$\mu_{sat} = \rho_b V_S^2$$
 (4)

Equations (1) and (3) are applicable for elastic waves propagating in elastic media.

Porous rocks are not strictly elastic due to which seismic waves are attenuative and dispersive (Müller et al., 2010), and therefore more complicated. But for practical purposes, equations (1) and (3) are assumed to be valid. Usually, laboratory measurements or log data are used to estimate the rock frame bulk and shear moduli, the grain density, porosity, and fluid bulk modulus, which are the parameters required for use of Gassmann's equations (Gassmann, 1951, 2007).

To determine the properties of different rocks, we need to determine, (1) the fraction by volume of various constituents, (2) elastic moduli of various phases, and (3) geometric details of how the phases are arranged relative to one another. Typically, information on internal geometry is not available. If we have information on the volume fraction of the constituents and their elastic moduli, we can only calculate the upper and lower bounds of the elastic moduli, and the elastic velocities of the composite rocks.

Voigt (1928) suggested that the upper bound on the effective elastic modulus of a mix of N material phases is given as

$$M_{\rm V} = \sum_{i=1}^{N} f_i M_i \tag{5}$$

where f_i is the volume fraction of the i^{th} constituent, and M_i is the elastic modulus of the i^{th} constituent.

Ruess (1929) gave the lower bound of the elastic modulus as

$$\frac{1}{M_{\rm R}} = \sum_{i=1}^{N} \frac{f_i}{M_i} \,, \tag{6}$$

where M represents the bulk or shear modulus.

To understand the variation of $V_{\rm P}$ as a function of porosity of say water-saturated sediments, we can refer to Figure 2.

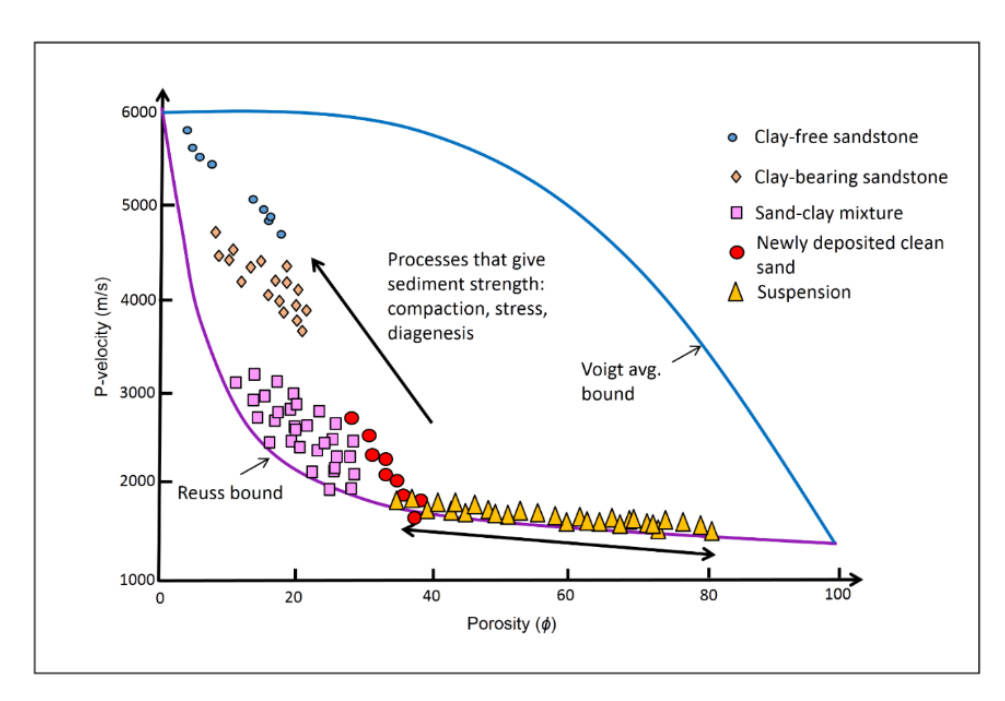


Figure 2: P-wave velocity plotted as a function of porosity for a variety of water-saturated sediments, compared with the Voigt-Reuss bounds. Data from Yin (1992), Han (1986) and Hamilton (1956). (After Avseth et al., 2005, and adapted from Chopra and Castagna, 2014)

Some of the observations that can be made from the above figure are as follows.

- 1. When the particles are suspended in water, their acoustic properties must fall on the Reuss average of mineral and fluid moduli.
- 2. When particles are deposited on the waterbottom, their properties still lie on or slightly above the Reuss average as long as they are weak and unconsolidated. The porosity of these particles will depend on the geometry of the particle stacking. Clean, well-sorted sands will be deposited with porosities near 40%. Poorly sorted sands will have lower porosities and will be deposited along the Reuss bound (Figure 2) Chalk will be deposited at high initial porosity of 55-65%. Shales can have even higher initial porosities. As these sediments get buried, different processes set in such as effective stress, compaction, cementing, and these move the sediments off the Reuss bound. The porosity at which the rock starts to become lithified and develop rigidity is called the critical porosity.
- 3. With increasing diagenesis, the moduli move further above the Reuss bound.
- 4. Sometimes the bounding methods are not seen as very helpful as the upper and lower bounds are well separated between the end members. In such cases, the critical porosity seems to help as it separates the fluid-bearing suspensions from the load-bearing frame.

Hashin-Shtrikman bounds (Hashin and Shtrikman, 1963) can be used to calculate the narrowest possible range for the bulk and shear modulus components in the absence of geometric details of how different phases of a rock are arranged relative to one another. They would therefore lie within the Voigt and Reuss bounds.

GASSMANN'S EQUATIONS

When a seismic wave passes through a porous saturated rock, the pore fluid contributes to the rock resistance to compression (incompressibility). Gassmann's equations mechanically relate the bulk modulus of the saturated rock ($\kappa_{\rm sat}$) to the bulk moduli of the pore fluid ($\kappa_{\rm f}$), the non-porous solid material comprising the rock ($\kappa_{\rm m}$) and the porous rock frame ($\kappa_{\rm drv}$).

$$\frac{\kappa_{\text{sat}}}{\kappa_{m} - \kappa_{\text{sat}}} = \frac{\kappa_{\text{dry}}}{\kappa_{m} - \kappa_{\text{dry}}} + \frac{\kappa_{\text{f}}}{\phi(\kappa_{m} - \kappa_{\text{f}})}, \tag{7}$$

and

$$\mu_{\rm m} = \mu_{\rm sat} \,. \tag{8}$$

where ϕ is the porosity, $\mu_{\rm m}$ is the shear modulus of the rock skeleton and μ_{sat} is the shear modulus of rock with pore fluid. Equation (7) is elegant in its symmetry and reveals that, for a given frame modulus, the higher the porosity the smaller the fluid effect. This is contrary to the observation that higher porosity rocks have larger fluid effects. The explanation for this apparent discrepancy is that the large fluid effect in high porosity rocks is entirely due to the low frame bulk modulus associated with high porosity. (A highly porous but incompressible rock frame would have a smaller fluid effect than a low porosity but equally incompressible rock frame). From this reasoning, it can be concluded that for a given porosity, a low aspect ratio pore structure will have a larger fluid effect than spherical pores. It is worthwhile pointing out that equation (7) is poorly behaved as porosity approaches zero and as the frame modulus approaches the solid grain modulus. This results in very inaccurate fluid substitutions in low porosity rocks as small errors in the porosity and other parameters are greatly magnified.

The derivation of Gassmann's equations assumes that (a) as the medium is deformed, there is enough time for the pore pressure to equilibrate throughout the interconnected pore space, (b) all the pores are in communication, (c) the rock frame is chemically and physically inert, (d) the rock is isotropic and homogeneous, (e) the rock is monomineralic and saturated with a single fluid, (f) there is no cavitation, and the pore fluid remains coupled to the solid material, and (g) the rock system is closed; there is no fluid flow in or out of the rock. It is possible that some of these assumptions are not strictly valid for the study at hand, but the results are usually reasonable, if not spectacular.

HERTZ-MINDLIN THEORY

The elastic moduli of a dry sand at critical porosity can be modeled as an elastic sphere pack, which is subjected to confining stress. As per the Hertz-Mindlin theory (Mindlin, 1949), for an identical spherical packing of grains with a critical porosity ϕ_c (equivalent to a well-sorted sand) and average number of contacts per grain

as n, subject to hydrostatic pressure, P, the bulk modulus can be given as

$$\kappa_{HM} = \left[\frac{n^2 (1 - \phi_c)^2 \mu_m^2}{18\pi^2 (1 - \nu_m)^2} P \right]^{1/3}, \tag{9}$$

and the shear modulus is given as

$$\mu_{HM} = \frac{5 - 4\nu}{5(2 - \nu_m)} \left[\frac{3n^2 (1 - \phi_c)^2 \mu_m^2}{2\pi^2 (1 - \nu_m)^2} P \right]^{1/3},\tag{10}$$

where $\kappa_{\rm m}$, μ_m = mineral bulk and shear moduli, ν_m = mineral Poisson's ratio. The above analysis assumes that there is no cement at the grain contacts, and if cement is present, it is deposited away from them. Dvorkin and Nur (1996) considered the addition of cement to the grains, which have the effect of reducing the porosity and enhancing the moduli of the aggregate.

The effective pressure can be calculated as the overburden pressure at a given depth, and the average number of contacts per grain, n, depends on the porosity and can be approximated by the following empirical equation (Murphy, 1982)

$$n = 20 - 34\phi + 14\phi^2. \tag{11}$$

When $\phi_c = 0.4$, n = 8.6, which is what is generally used in the computations.

To calculate the values of the effective bulk and shear moduli for a dry frame at a different porosity (ϕ , other than the critical porosity), the Hashin Shtrikman lower bound is utilized and the following expressions can be derived.

$$\kappa_{dry} = \left[\frac{\phi/\phi_c}{\kappa_{HM} + (^4/_3)\mu_{HM}} + \frac{1 - ^\phi/\phi_c}{\kappa_m + (^4/_3)\mu_{HM}} \right]^{-1} - \frac{4}{3}\mu_{HM}, \tag{12}$$

$$\mu_{dry} = \left[\frac{\phi/\phi_c}{\mu_{HM} + z} + \frac{1 - \phi/\phi_c}{\mu_{HM} + z} \right]^{-1} - z,$$

where
$$z = \frac{\mu_{HM}}{6} \left(\frac{9\kappa_{HM} + 8\mu_{HM}}{\kappa_{HM} + 2\mu_{HM}} \right)$$
, (13)

The saturated elastic moduli, $\kappa_{\rm sat}$, and $\mu_{\rm sat}$ can be calculated with the use of Gassmann's equations described above.

Finally, the density needs to be calculated which can make use of the following relationship.

$$\rho_b = \phi \rho_f + (1 - \phi) \rho_m \tag{14}$$

where ρ_f is the fluid density, and ρ_m is the mineral density.

Now that the moduli and density are determined as a function of porosity and fluid saturation, P- and S-velocities can be computed using equations (1) and (3). Finally, the crossplot between P-impedance and $V_P V_S$ is plotted and is discussed next.

GENERATION OF ROCK PHYSICS TEMPLATES (RPTs)

Odegaard and Avseth (2003) introduced a rock physics template comprising the acoustic impedance versus V_PV_S crossplot which allows the estimation of fluid and lithology content of a reservoir. As was discussed above, this was done by combining the depositional and diagenetic trend models with Gassmann's fluid substitution, and entails the following steps:

- Using the Hertz-Mindlin theory for computing the moduli of the dry rock frame at critical porosity.
- Using the lower Hashin-Shtrikman bound for computing the moduli of the dry rock frame over a range of porosities.
- 3. Using Gassmann's equations for performing fluid substitution.
- 4. Using the computed moduli to compute the densities and velocities which result in the evaluation of $V_P V_S$ and acoustic impedance which are then crossplotted.

Such templates can be constructed for areas of interest, for understanding better, lithology, mineralogy, water depth, burial depth, pressure and temperature gradients, diagenesis and fluid properties. They help in risk reduction in seismic exploration and prospect evaluation.

RPT provides a quick and efficient way of interpreting seismic inversion results and predicts reservoir properties where there is no well control. With the assumption that the undrilled area has the same depositional environment, quantitative estimation of reservoir parameters like porosity, saturation, cement volume, etc. can be made. However, the success of such extrapolation depends on the accuracy of the rock physics models and the knowledge of the reservoir geology.

GEOHORIZONS, Vol. 30, No. 1, June 2025 © SPG India. All rights reserved.

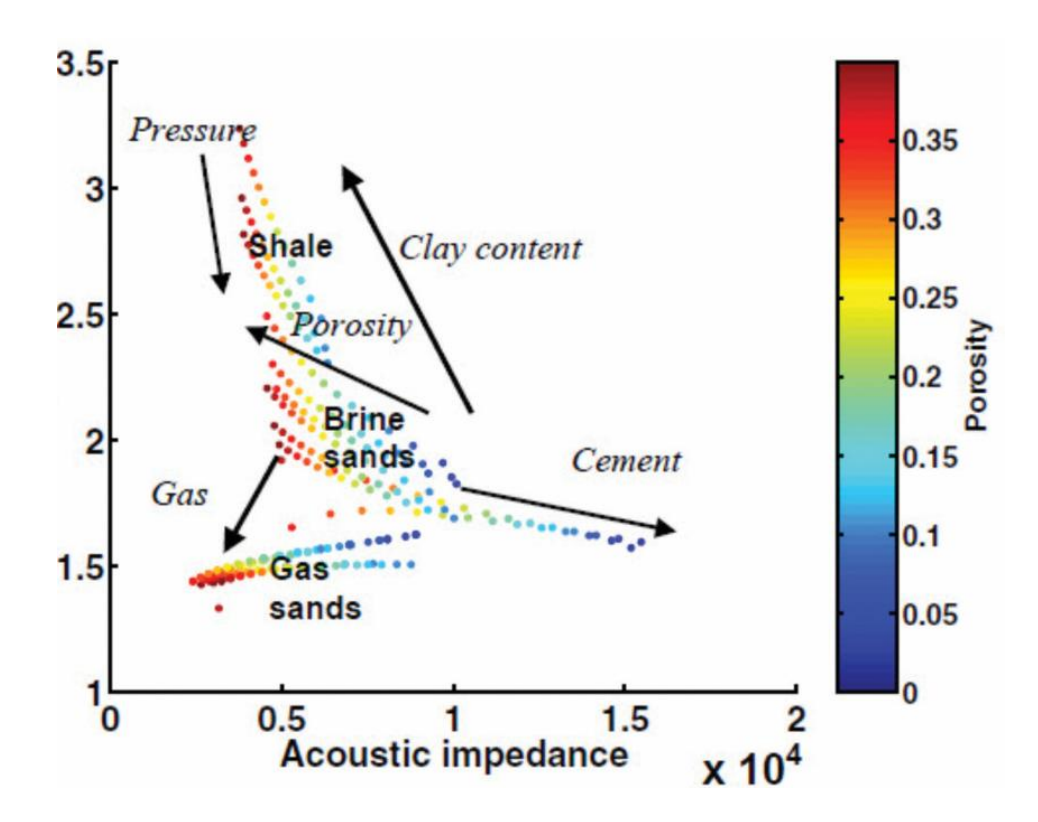


Figure 3: Interpretation of a rock physics template in terms of mineralogy, fluid content, cementation, pressure and clay content (After Ødegaard and Avseth, 2003).

During deposition, sands exhibit very high $V_P V_S$ ratios when saturated with water, as the shear modulus is significantly reduced at low effective pressure. As burial depth increases, the sands will undergo mechanical compaction. With grain crushing and tighter packing, both V_P and density (and thus impedance) will rise. As pressure increases at the grain contacts, both V_P and V_S will increase, while the V_PV_S ratio will decrease. At a certain depth and temperature, chemical compaction will begin, and the rock frame will become cemented. This cementation at grain contacts further lowers the V_PV_S ratio, while impedance increases. As a result, the water-saturated sandstone, which may initially have a porosity of 40% at deposition and eventually reach zero porosity with pure solid material, will follow a non-linear trend on the RPT of acoustic impedance versus V_PV_S , as illustrated in Figure 3.

As the clay content in a sandstone increases, the acoustic impedance also increases, particularly when clay particles fill the pores. However, when clay is present in laminations, such as fine layers of clay alternating with sandstone layers, an increase in GEOHORIZONS, Vol. 30, No. 1, June 2025 © SPG India. All rights reserved.

shaliness results in a decrease in acoustic impedance. Laminated clay has a greater impact on the V_P/V_S ratio compared to pore-filling clay. The presence of laminated clay significantly weakens the sandstone's rock frame, leading to a large decrease in shear velocity (V_S), whereas pore-filling clay has minimal effect on shear modulus but increases the bulk modulus (leading to a rise in V_P). In both scenarios, increasing clay content causes V_P to rise.

In the presence of hydrocarbons, the bulk modulus and density decrease compared to the water-saturated case, while the shear modulus remains unaffected. As a result, both acoustic impedance and $V_{\rm P}V_{\rm S}$ decrease with increasing hydrocarbon saturation.

Fluid sensitivity is higher in relatively soft rocks, which typically have high porosities, than in stiffer rocks, which are generally associated with lower porosities.

As discussed by Avseth and Veggeland (2015), the following may serve as a general guideline on RPTs. An oil-saturated sandstone and brine-saturated sandstone, both having similar porosity will overlap on the RPT

(Impedance versus $V_P V_S$), and this overlap can be larger for well-consolidated sandstones with relatively small fluid sensitivity, i.e. fluids may not cause swelling and influence permeability and strength of the sandstone. A clean, cemented sandstone with brine can have lower V_PV_S than an unconsolidated sand filled with oil. Gassaturated sandstones may have V_P/V_S ratios between 1.5 and 1.6, and they will be normally well-separated from water-saturated sandstones unless the rocks are very tight. Sandstones with normal porosity (of 10 to 20 %), filled with light oil and those filled with water will overlap. Similarly, sandstones with homogeneous lowgas saturation and those with commercial gas saturation will overlap. In the case of patchy saturation, a linear drop in both V_PV_S and impedance will be seen with increasing saturation.

APPLICATIONS

Based on the available log data, the software (commercial/open-data base) one is using for the generation of the RPTs usually offers the choice for the models that the user can make, which will also depend on the complexity of the reservoir.

We demonstrate the RPT generated for an area in the Lower Magdalena Valley (LMV) Basin located onshore in northwest Colombia. The main reservoir sands are found in the upper part of the Late Miocene age formation deposited in a fluvial to deltaic to shallow marine environment. The generated RPT in the broad interval of interest is shown in Figure 4.

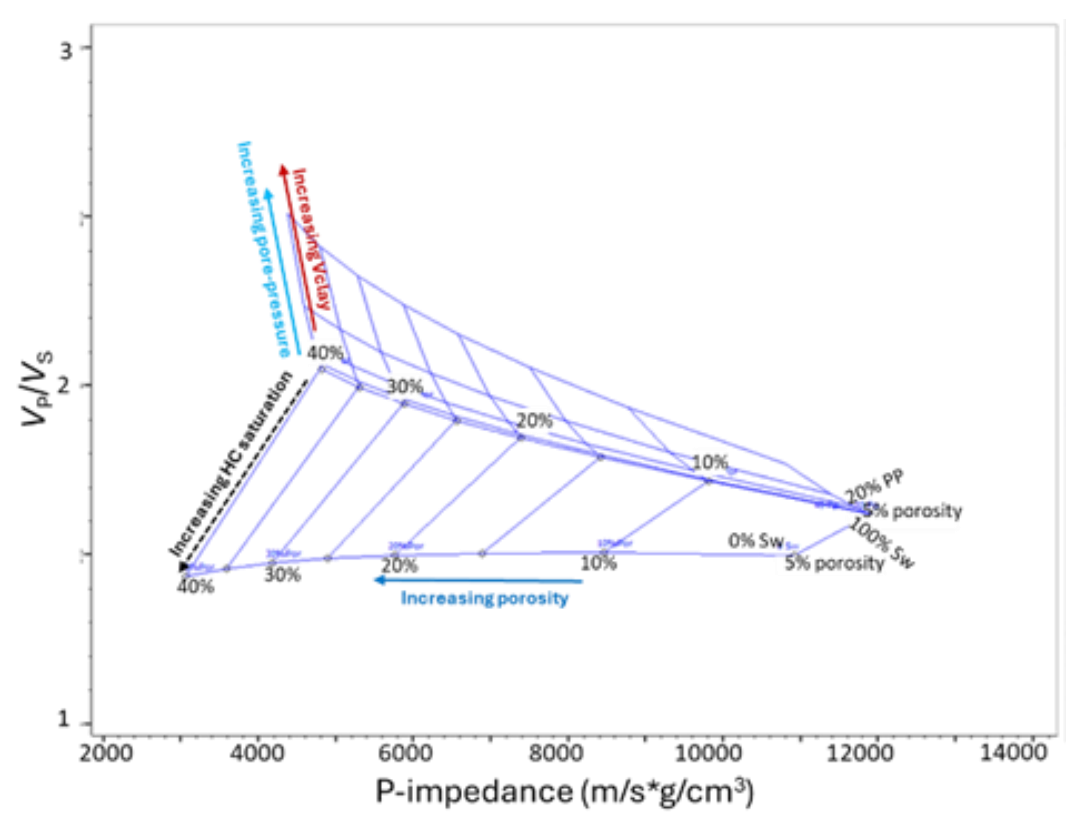


Figure 4: An RPT showing the combined variation of porosity, water-saturation, volume of clay and pore-pressure. The variations of different properties can be seen in different directions. Once this template is overlaid on well or seismic data the data points in different clusters can be interpreted as coming from the background lithology, and those that are associated with lithologies of interest impregnated with hydrocarbons, and thus more interesting.

In addition to the procedure followed for generating an RPT as explained earlier, for the pore pressure segment, the pressure data available for some wells was used. Using the determined range of values in the interval of

interest, and using a gradient of 23 MPa/km, the average values of pore pressure and total pressure used for generating the template were 30 and 48 MPa, respectively.

GEOHORIZONS, Vol. 30, No. 1, June 2025 © SPG India. All rights reserved.

The well data for P-impedance and V_P/V_S were crossplotted on the generated template in Figure 4 and is depicted in Figure 5. The cluster points are colour-

coded with water-saturation. Notably, the cluster points seem to be falling within the range of known porosity and S_w , which is encouraging.

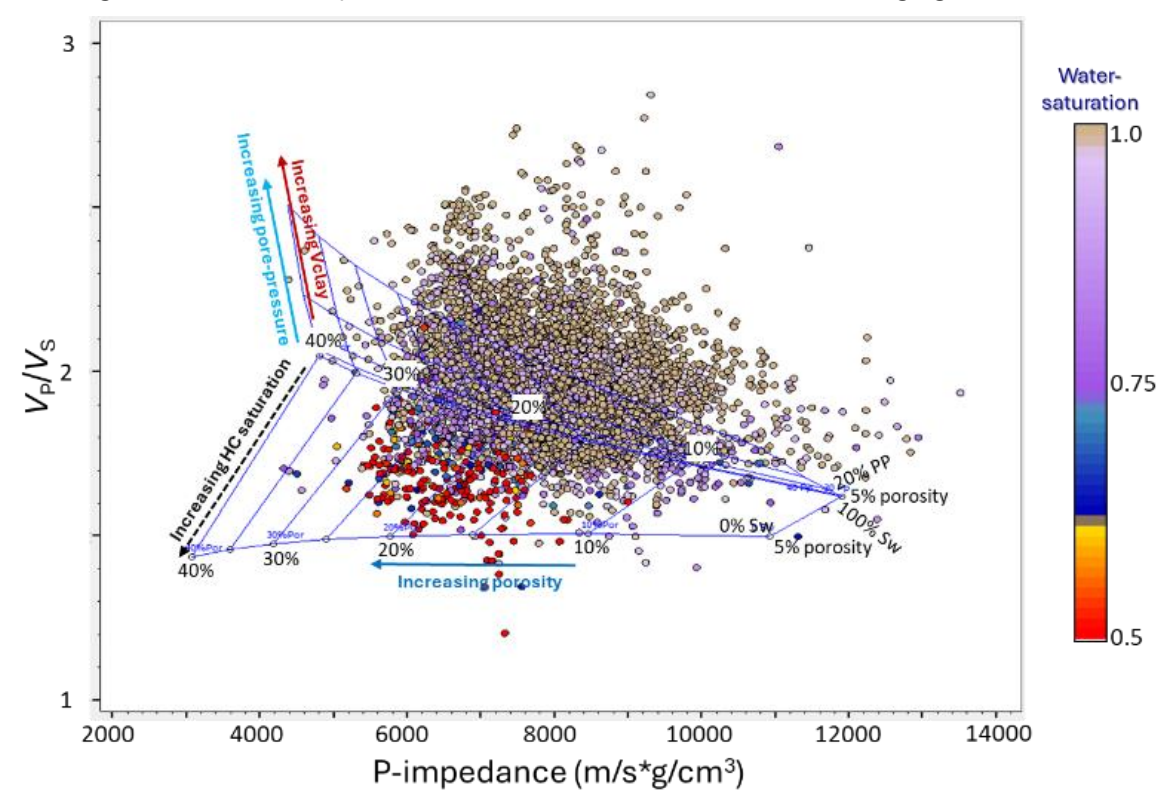


Figure 5: Calibrated RPT generated for the interval of interest using well data from a few wells showing the effect of porosity, water-saturation and pore pressure It is overlaid by the well data points corresponding for P-impedance and V_PV_S . The RPT seems to follow the data points very well (i.e. the cluster points are falling within the range of known porosity and Sw). The cluster points are colour-coded with water-saturation.

We now examine the application of the generated RPT and highlight its advantages over a purely qualitative interpretation, particularly in the context of the fluid factor attribute volume. This attribute is commonly employed to emphasize anomalous zones potentially indicative of hydrocarbons (Kumar et al., 2024). Figure 6a displays a crossline section extracted from the fluid factor volume, overlaid with the water saturation curve. While the attribute successfully highlights anomalies associated with two sand units (indicated by yellow and cyan arrows), it lacks the ability to quantitatively differentiate between them—specifically, whether both sands are of comparable reservoir quality or if they differ in porosity and saturation.

In contrast, the RPT provides a quantitative framework for such differentiation. Figure 6b presents a crossplot of inverted P-impedance versus V_PV_S ratio across a broad area of interest, with the RPT overlaid to delineate regions corresponding to varying porosity and fluid saturation conditions. Cluster points are identified and enclosed within ellipses based on their elastic properties. These clusters are then back-projected onto a vertical seismic section intersecting a well (Figure 6c), allowing spatial visualization of lithofacies and fluid distribution. A comparison between Figures 6a and 6c demonstrates the added value of the RPT: although both sand units show fluid factor anomalies, only the upper sand is associated with higher porosity, while the lower sand is identified as relatively tight.

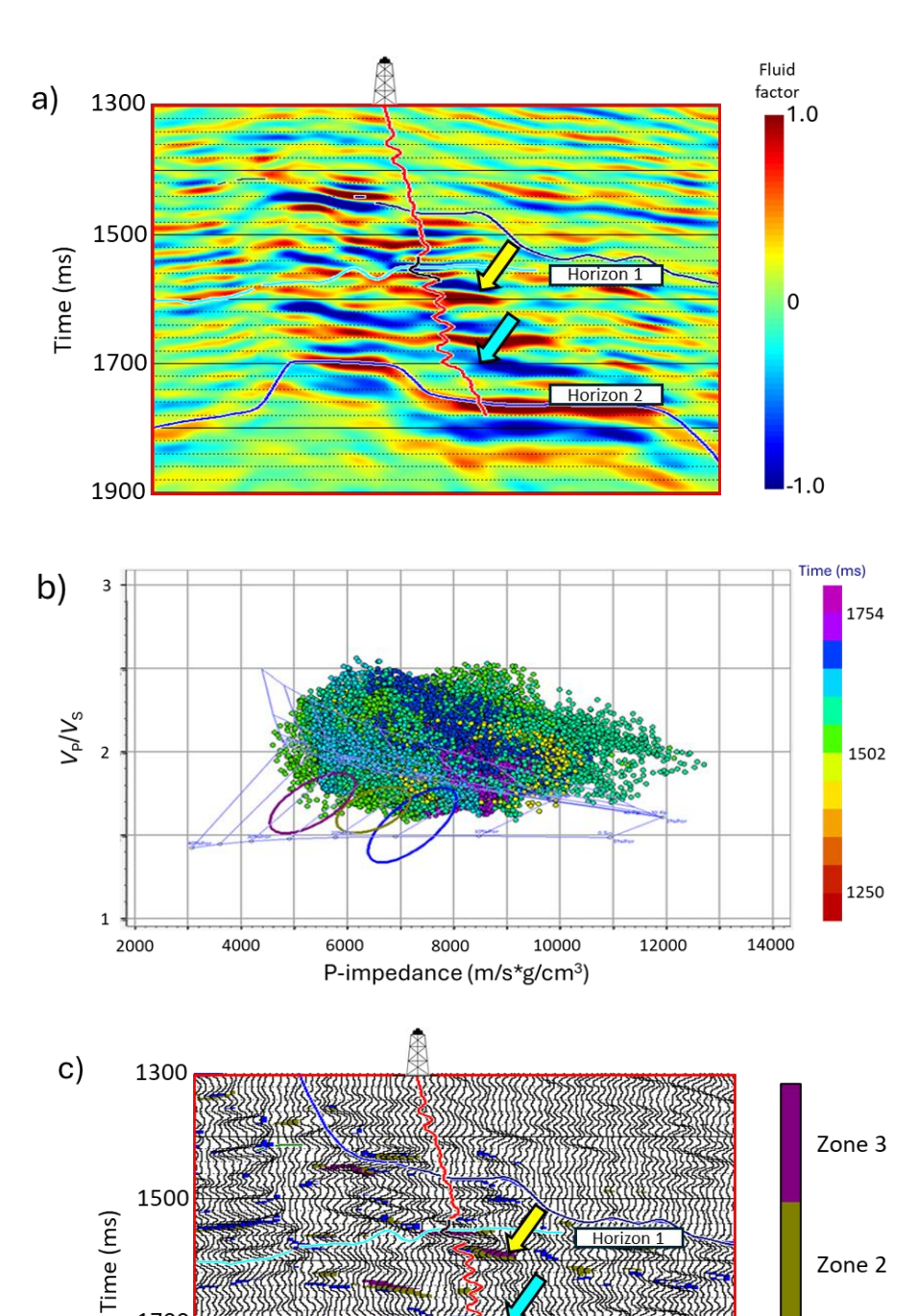


Figure 6: (a) A segment of a crossline section extracted from the fluid factor attribute volume passing through a well, with the water-saturation curve in red shown overlaid on it. The anomalies for two sands are seen at the location of the yellow and cyan block arrows. (b) An RPT is generated for P-impedance and V_PV_S attributes derived from seismic data. Three ellipses are drawn on the template which are expected to highlight hydrocarbon effect. (c) The cluster points enclosed by the ellipses drawn in (b) are backprojected on the vertical section passing through the well, and it shows some pockets that exhibit those values. Interestingly, it highlights the sands indicated with the yellow and cyan block arrows.

Figure 7a provides a further example where the fluid factor suggests an anomaly that was targeted by drilling. However, post-drill analysis revealed no hydrocarbon GEOHORIZONS, Vol. 30, No. 1, June 2025 © SPG India. All rights reserved.

1700

presence, as confirmed by the water saturation curve. When the RPT-derived clusters from Figure 6b are back-projected onto the corresponding vertical section

Zone 1

(Figure 7b), no zones matching favorable rock and fluid conditions are observed. This illustrates the critical role of the RPT in validating or de-risking seismic anomalies. Had the RPT analysis been conducted prior to drilling, the unproductive well could likely have been avoided.

Thus, while qualitative displays may appear convincing, the RPT enables a more robust, quantitative interpretation of seismic attributes in relation to reservoir properties.

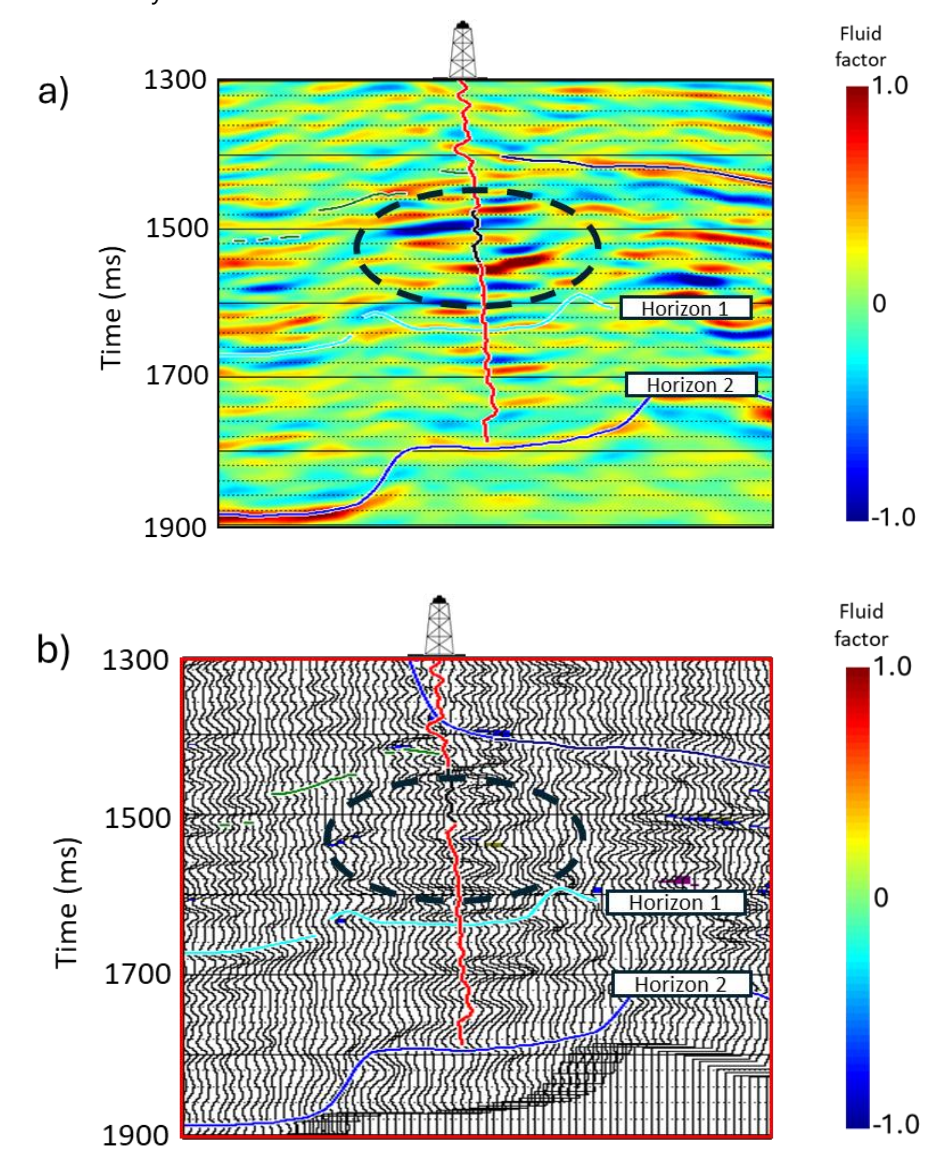


Figure 7: (a) A different segment of a crossline section, extracted from the fluid factor attribute volume, is shown intersecting a well. The water saturation curve (in red) is overlaid on this section. A few sand anomalies are visible within the highlighted area. When the RPT-derived clusters from Figure 6b were back-projected onto the corresponding vertical section (Figure 7b), a few small, localized zones that match the expected attribute values are seen but no zones matching favorable rock and fluid conditions are observed. Notably, the region enclosed by the dashed black ellipse is not highlighted, indicating it does not share the same characteristics.

CONCLUSIONS

The RPTs described in this tutorial for the impedance versus $V_P V_S$ plots are a valuable aid for interpretation of GEOHORIZONS, Vol. 30, No. 1, June 2025 © SPG India. All rights reserved.

well data in terms of lithology and fluid content. When overlaid on seismically derived P-impedance versus

 V_PV_S attributes, these templates enable effective interpretation and classification. Consequently, seismic AVO inversion followed by RPT analysis should constitute an essential part of all interpretation exercises.

RPTs can be generated by selecting appropriate parameter ranges, as discussed earlier in the article. In

ACKNOWLEDGEMENTS

The authors would like to express their sincere gratitude to Per Avseth for graciously agreeing to review this tutorial article. His expert insights ensured that no finer details were overlooked, significantly enhancing the clarity and overall readability of the tutorial.

the case study presented, the RPT analysis validated one

set of anomalies identified from the fluid factor attribute,

which guided the drilling of a well. However, a second

well, drilled under similar assumptions failed to deliver the expected results, likely due to the absence of RPT

analysis at the time. This underscores the potential of

RPTs as a critical interpretive tool and supports their

routine use in exploration and development efforts. (?

REFERENCES

Avseth, P., T. Mukerji, and G. Mavko, 2005, Quantitative seismic interpretation, Cambridge University Press.

Avseth, P. and T. Veggeland, 2015, Seismic screening of rock stiffness and fluid softening using rock-physics attributes, Interpretation, **3**(4), SAE85-SAE93. https://doi.org/10.1190/INT-2015-0054.1

Avseth, P., 2025, Personal communication.

Chopra, S. and J. P. Castagna, 2014, AVO, SEG Investigations in Geophysics Series, No. 16.

Chopra, S., R. K. Sharma, G. K. Grech, and B. E. Kjølhamar, 2017, Characterization of shallow high-amplitude seismic anomalies in the Hoop Fault Complex, Barents Sea, Interpretation, **5**(4), T607–T622. http://dx.doi.org/10.1190/INT-2017-0054.1.

Dvorkin, J. and A. Nur, 1996, Elasticity of high-porosity sandstones: Theory for two North Sea data sets, Geophysics, **61**(5), 1363-1370. https://doi.org/10.1190/1.1444059

Gassmann, F., 1951, Elasticity of porous media: Uber die Elastiz-itat poroser Medien: Vierteljahrsschrift der Naturforschenden Ges-selschaft in Zurich, Heft 1.

Gassmann, F., 2007, Elasticity of porous media, Geophysics Reprints Series:389-408.

https://doi.org/10.1190/1.9781560801931.ch3p

Hamilton, E. L., 1956, Low sound velocities in high porosity sediments, J. Acoust. Soc. Am., **28**, 16-19. https://doi.org/10.1121/1.1908208

Han, D., 1986, Effects of porosity and clay content on acoustic properties of sandstones and unconsolidated sediments, unpublished Ph.D. thesis. Stanford University.

Hashin, Z., and S. Shtrikman, 1963, A variational approach to the elastic behavior of multiphase materials, J. Mech. Phys. Solids, **11**(2),127-140. https://doi.org/10.1016/0022-5096(63)90060-7

Kumar, N., R. K. Sharma, S. Chopra and N. Ganguly, 2024, Seismic pitfalls: impact of converted waves on AVO; how to recognize and avoid them, GEOHORIZONS, **29**(1), 95-104.

Mavko, G., T. Mukerji, and J. Dvorkin, 2009, The Rock Physics Handbook 2nd ed. (New York: Cambridge University Press)

Mindlin, R. D., 1949, Compliance of elastic bodies in contact, J. Appl. Mech., **16**(3), 259-268.

https://doi.org/10.1115/1.4009973

Müller, T. M., B. Gurevich and M. Lebedev, 2010, Seismic wave attenuation and dispersion resulting from wave-induced flow in porous rocks — A review, Geophysics, **75**(5), A147-A164. https://doi.org/10.1190/1.3463417

Odegaard, E. and P. Avseth, 2003, Interpretation of elastic Inversion Results Using Rock Physics Templates, 65th EAGE Conference and Exhibition, Expanded abstract, E17. https://doi.org/10.3997/2214-4609-pdb.6.E17

Reuss, A. (1929) Berechnung der Fliessgrenze von Mischkristallen auf Grund der Plastizitätsbedingung für Einkristalle. ZAMM—Journal of Applied Mathematics and Mechanics/Zeitschrift für Angewandte Mathematik und Mechanik. **9**, 49-58.

http://dx.doi.org/10.1002/zamm.19290090104

Voigt, W., 1928, Lehrbuch der Kristallphysik (mit ausschluss der krystaloptik) [Textbook on crystal physics], reprint of the first edition, published in 1910:Teubner. https://doi.org/10.1007/978-3-663-15884-4

Yin, H., 1992, Acoustic velocity and attenuation of rocks: Isotropy, intrinsic anisotropy, and stress induced anisotropy, Ph.D. thesis, Stanford University.

GEOHORIZONS, Vol. 30, No. 1, June 2025 © SPG India. All rights reserved.



Satinder Chopra is the founder and President of SamiGeo Consulting Ltd., based in Calgary. He has 40 years of experience as a geophysicist specializing in processing, special processing, and interactive interpretation of seismic data. His research interests focus on techniques aimed at characterization of reservoirs. He has published nine books and more than 525 papers and abstracts. His work and presentations have won several awards from international professional societies the most notable ones being the Roy O. Lindseth CSEG Medal Award (2021), Lifetime Membership Award (2021) by Petroleum History Society, AAPG Honorary Membership Award (2024), AAPG Distinguished Service Award (2019), EAGE Honorary Membership (2017), CSEG Honorary Membership (2014), CSEG Meritorious Service (2005) Award, 2014 APEGA Frank Spragins Award, the 2010 AAPG George Matson Award, and the 2013 AAPG Jules Braunstein Award. He has been the 2010/11 CSEG Distinguished Lecturer, the 2011/12 AAPG/SEG Distinguished Lecturer, and the 2014/15 EAGE e-Distinguished Lecturer.



Dr. Ritesh Kumar Sharma received his master's and Ph.D. degrees in geophysics from the University of Calgary. He has worked as senior reservoir geoscientist at TGS, Canada till 2020, and now works for SamiGeo Consulting Ltd. at Calgary. Ritesh has vast experience in working with applications such as AVO analysis (including azimuthal AVO), rock-physics analysis, frequency enhancement of seismic data, simultaneous inversion, extended elastic impedance inversion as well as geostatistical inversion. He has won the best poster award for his presentation at the 2012 GeoConvention held at Calgary, the Jules Braunstein Memorial Award for the best AAPG poster presentation at the 2013 AAPG Convention held at Pittsburgh, CSEG Honorable Mention for the Best Recorder Paper award in 2013 and is the recipient of Honorable Mention Best Poster Paper in SEG 2017. He is an active member of SEG and CSEG.



Neeraj Kumar has over twenty years of experience in petroleum exploration and development. He received his M.Tech. in applied geophysics from erstwhile University of Roorkee (now known as IIT Roorkee), in 1999. Presently, he serves as the Senior Geophysical Advisor at Canacol Energy in Calgary, Canada. His previous roles include positions at Cairn Energy, Mubadala, and Petronas. Neeraj's areas of expertise include seismic interpretation, prospect evaluation, the integration of geophysical and geological data, volumetrics, geological risking, and project management.